Theor Chem Acc (2011) 129:381–387
DOI 10.1007/s00214-010-0856-x

REGULAR ARTICLE

Theoretical study of the interaction between Pt(0) and MPH_3^+ fragments in complexes of the $[Pt_3\ (\mu\text{-}CO)_3(PH_3)_3]$–$MPH_3^+$ (M = Cu^+, Au^+, Ag^+) type

Daniela Donoso · Fernando Mendizabal

Received: 13 September 2010 / Accepted: 8 November 2010 / Published online: 23 November 2010
© Springer-Verlag 2010

Abstract Ab initio calculations suggest that a series of complexes of the $[Pt_3(\mu\text{-}CO)_3(PH_3)_3]$–$MPH_3^+$ type (M = Cu, Au, Ag) are stable. We have studied these complexes at the HF, MP2, B3LYP, and PBE levels of theory. The magnitude of the interaction energies and Pt_3–M distances indicate a substantial covalent character of the bond, the latter being confirmed by orbital diagrams. The chemical bond is sensitive to electron correlation effects. In addition, the Fukui index of nucleophilic attack and electrophilicity index on the metal were used to explore possible sites where chemical reactivity may play a role.

Keywords Platinum clusters · Metallic interactions · Coin metals

1 Introduction

Since the 1960s, the chemistry of clusters has produced varied complex structures, the most widely studied of which are triangular trimetallic units, M_3 [1]. For several years, the cluster chemistry of Pt(0) in particular has had considerable appeal: synthetic [2], structural, [3] and spectroscopic [4] studies on a large number of clusters containing Pt_3 units have been reported, including structures that have been characterized [5] by IR, NMR, and X-rays.

A metal cluster is group of metal atoms bound directly to each other. A metal cluster can be isolated (naked) or associated with a given number of ligands [6]. The molecular clusters can be classified according to the presence and nature of the ligand, which can be a bridging ligand or terminal ligand. Some of the most frequently used techniques to elucidate the structure of clusters are X-ray crystallographic studies [5, 6], nuclear magnetic resonance (NMR), and infrared spectroscopy [6–8]. As mentioned earlier, the triangular trimetallic structure M_3 can react as Lewis bases or acids [1]. The elements of the triad of nickel form these complexes with a triangular metal framework.

Heterometallic clusters with Pt_3 have received a lot of attention in homogeneous and heterogeneous catalysis [9]. A particularly versatile block is $[Pt_3(\mu\text{-}CO)_3(PR_3)_3]$ [10], because it shows HOMO–LUMO heterometallic between the triplatinum and the other metal units, giving the cluster both σ-donor and weak π-acceptor properties. Thus, this $[Pt_3(\mu\text{-}CO)_3(PR_3)_3]$ (R = $-PCy_3$;$-PPh_3$) cluster can form two "sandwich-like" and other "half-sandwich-like" heterometallic clusters with Cu, Ag, and Au [1, 11]. The type of the interaction is d^{10}–d^{10} between Pt_3 core and coin metal. The interactions have been theoretically described first time by Pekka Pyykkö [12, 13]. When the $[Pt_3(\mu\text{-}CO)_3(PR_3)_3]$ cluster reacts with two Hg atoms, it forms the sandwich type. It can also react with donors like PR_3 and CO [14].

The electronic and structural features of triangular platinum clusters have been studied by extended Hückel molecular orbital theory (EHT) calculations [15]. The cluster-bonding orbitals at the EHT level are markedly stabilized by edge-bridging ligands. In the $[Pt_3(\mu\text{-}CO)_3(PH_3)_3]$–$AuPH_3^+$ models, the $AuPH_3^+$ fragments cap the Pt_3 triangles by utilizing the acceptor orbital of a_1 symmetry localized on gold [16, 17]. To our knowledge, no

Dedicated to Professor Pekka Pyykkö on the occasion of his 70th birthday and published as part of the Pyykkö Festschrift Issue.

D. Donoso · F. Mendizabal (✉)
Departamento de Química, Facultad de Ciencias,
Universidad de Chile, Casilla 653, Santiago, Chile
e-mail: hagua@uchile.cl

ab initio studies at a higher level have been reported for the systems presented in this study.

We have predicted a number of stable complexes of the type $[Pt(PH_3)_3–M(PH_3)]^+$ (M = Cu, Ag, Au) [18] based on ab initio calculations at HF, MPn ($n = 2, 4$), CCSD, CCSD(T), B3LYP, and PBE0 levels of theory. These complexes exhibit a strong closed shell d^{10}–d^{10} interaction; the magnitudes of the interaction energies are in the ranges of 198 (HF) and 251 kJ/mol (B3LYP), magnitudes associated with covalent bonds [19]. Concluding that the equilibrium distances and interaction energy are sensitive to the electronic correlation potential, the interaction is mainly orbital driven, with a strong dipole induced and dispersion component present.

Many efforts have been made to obtain some generalizations that allow us to rationalize experimental features such as structure and reactivity, and also the implementation of quantitative theoretical calculations. Therefore, the interest of this work is to study the structure, binding properties, and reactivity of these triangular platinum clusters, Pt_3, in addition to predicting the reactivity of the system through the frontier orbitals by analysing the Hard/Soft–Acid/Base principle [20], applying the density functional theory (DFT) concept [21–24].

2 Models and computational methods

A simplified model of the experimental structures with the general formula of $[Pt_3(\mu\text{-}CO)_3(PPh_3)_3]–MPPh_3^+$ (M = Au, Ag, Cu) is depicted in Fig. 1. The structure assumes C_{3v} point symmetry. In order to keep the computations feasible, we use phosphine (PH_3) instead of the original triphenylphosphine ligands. Although it has been shown that there are deviations from experimental values used at high level as the CCSD(T) method [25]. Moreover, we have studied the $[Pt_3(\mu\text{-}CO)_3(PH_3)_3]$ complex and MPH_3^+ separately for the purpose of comparing the structures.

The theoretical studies have been carried out by ab initio calculations available in the Gaussian03 program [26] at the Hartree–Fock (HF), second-order Møller–Plesset perturbation theory (MP2) [27], B3LYP, and PBE [28]. The aim of including DFT calculations is to show that these systems with strong metal–metal interactions be described by DFT. This was demonstrated in $[Pt(PH_3)_3–M(PH_3)]^+$ (M = Cu, Ag, Au) [18, 19]. For the heavy elements Pt, Au, Ag, and Cu, the Stuttgart small-core pseudorelativistic effective core potentials (PP) were used: 18 valence electrons (VE) for Pt and 19 for Au, Ag, and Cu [29]. Two f-type polarization functions were added: Pt ($\alpha_f = 0.70, 0.14$), Au ($\alpha_f = 0.20, 1.19$), Ag ($\alpha_f = 0.22, 1.72$), and Cu ($\alpha_f = 0.24, 3.70$) [30]. The C, O, and P atoms were also treated with PP, using a

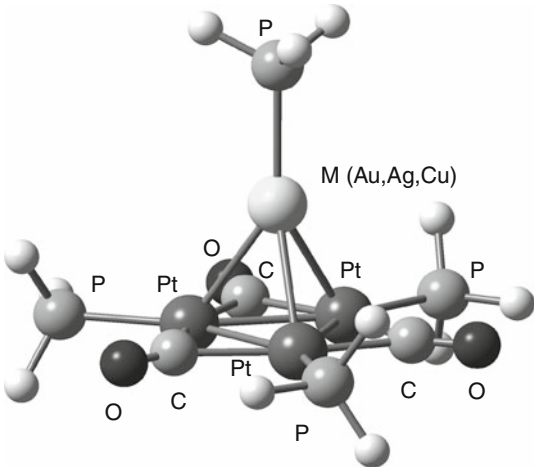

Fig. 1 The $[Pt_3(\mu\text{-}CO)_3(PH_3)_3]–MPH_3^+$ (M = Au, Ag, Cu) model

double-zeta basis set and adding one d-type polarization function [31]. For hydrogen, a valence-double-zeta basis set with one p-polarization function was used [32].

The counterpoise correction for the basis set superposition error (BSSE) was used for the calculated interaction energies. We have fully optimized the geometry of the model for each one of the methods mentioned previously.

With the aim of understanding the interaction of the electrophilic fragment MPH_3^+ (M = Au, Ag, Cu) with the $[Pt_3(\mu\text{-}CO)_3(PH_3)_3]$ cluster, we have used the conceptual density functional theory (CDFT). The chemical potential (μ) and chemical hardness (η) from operational DFT [21–24] are defined as:

$$\mu \cong -\frac{(IP + AE)}{2} \tag{1}$$

$$\eta \cong \frac{(IP - AE)}{2} \tag{2}$$

where IP is the ionization potential, and AE is the electron affinity. These two quantities can also be defined based on orbitals; on the basis of Koopmans' theorem as $IP \approx -E_{HOMO}$ and $AE \approx -E_{LUMO}$, where E_{HOMO} and E_{LUMO} are the energies of the highest occupied molecular orbital (HOMO) and lowest unoccupied molecular orbital (LUMO), respectively. On the other hand, the electrophilicity index (ω) is defined as [33]

$$\omega = \frac{\mu^2}{2\eta} \tag{3}$$

It is a measure of electrophilicity of the ligand and corresponds to a measure of electrophilic power. The higher its value, the greater its electrophilic ligand capacity. In addition, to see reactive sites, the Fukui local function [33] for electrophilic fragments was determined on a finite-difference basis by the gross natural charge (q) at *M*, where

M represents a metal atom in the fragment with $N + 1$ electrons. The Fukui index for nucleophilic attack is given as

$$f_{\mathrm{M}}^{+} = q_{\mathrm{M}}(N+1) - q_m(N) \quad (4)$$

Thus, a local electrophilicity has been introduced to analyze the electrophile–nucleophile reactions. It is defined as

$$\omega_{\mathrm{M}}^{+} = \omega f_{\mathrm{M}}^{+}. \quad (5)$$

3 Results and discussion

3.1 Structural description and bonding energies

We have assumed for all clusters a singlet ground state. The experimental data indicate that the clusters are diamagnetic [4–7]. Tables 1, 2, and 3 summarize the main geometric parameters and interaction energies obtained for the optimized geometries at several theoretical levels. The experimental values are taken from solid-state X-ray. The theoretical values are within the experimental ones. The magnitudes of MP2 are the shortest, followed by B3LYP and PBE.

As to the Pt–M distances and the interaction energy (see Table 3), it is clear that electronic correlation effects play an important role in the stability of the system. The Pt–M distances obtained with all methods are close to that of a typical single bond, with the shortest distance obtained with the MP2 method [15]. The same goes for M–P distances. In the case of gold fragments, Au–P distances of the electrophile increase slightly at all theoretical levels when the complex is formed [34, 35]. Also, the system's H–Pt–P angle shows less deviation compared with the free $[Pt_3(\mu\text{-}CO)_3(PH_3)_3]$, e.g. 117°–119° at MP2 level.

Table 1 Main geometric parameters of the $[Pt_3(\mu\text{-}CO)_3(PH_3)_3]$ complex (distances in pm and angles in degrees) at different levels of calculation

Complex	Method	Pt–Pt	Pt–P	P–H	C–O	HPPt°	OCPt°
$[Pt_3(\mu\text{-}CO)_3(PH_3)_3]$	HF	273.7	233.7	141.2	113.0	118.8	139.9
	MP2	261.9	226.1	142.0	117.7	118.8	140.7
	B3LYP	271.3	230.8	143.1	116.4	119.3	139.8
	PBE	268.7	228.8	144.6	117.8	119.8	139.9
$[Pt_3(\mu\text{-}CO)_3(PPh_3)_3]$[a] [5]	Exp	275.0	225.2		117.2		140.5
$[Pt_3(\mu\text{-}CO)_3(PCy_3)_3]$[b] [5]	Exp	265.5	227.5		117.5		140.3

[a] PPh_3 is triphenylphosphine

[b] PCy_3 is tricyclohexylphosphine

Table 2 Main geometric parameters of the MPH_3^+ fragment (M = Au, Ag, Cu)

Fragment	Method	M-P	P–H	HPM°
$AuPH_3^+$	HF	239.2	140.2	114.5
	MP2	225.1	140.9	113.1
	B3LYP	229.5	142.0	113.5
	PBE	226.6	143.5	113.3
$AgPH_3^+$	HF	260.9	140.6	116.4
	MP2	240.2	141.1	115.8
	B3LYP	243.9	142.2	115.9
	PBE	239.1	143.6	115.8
$CuPH_3^+$	HF	237.2	140.5	115.9
	MP2	217.7	141.0	115.4
	B3LYP	221.3	142.2	115.3
	PBE	217.8	143.6	115.3

Distances in pm and angles in degrees at different levels of calculation

The magnitude of the interaction energies obtained varies between 162 (HF) and 492 kJ/mol depending on the method and fragment used (MP2). Such magnitudes are generally associated with covalent bonds. This might be indicative of an orbital stabilization due to the formation of stable adducts between the $[Pt_3(\mu\text{-}CO)_3(PH_3)_3]$ and the $[MPH_3]^+$ fragments. The complexes are already stabilized at the HF level as shown in Table 3. A strong oscillation of the interaction energy is seen depending on the method used. It is clear that the electron correlation component plays an important role. When this term is included, an increased interaction energy is obtained.

In order to get a better insight into such stabilization, HF orbital energies for $[Pt_3(\mu\text{-}CO)_3(PH_3)_3]$–$MPH_3^+$ (M = Au, Ag, Cu) complexes with MP2 geometry have been depicted in Fig. 2. The frontier molecular orbital positions in the orbital energy spectra of the three complexes are very similar, with a HOMO-LUMO gap of approximately 7.7 eV for all the complexes. The energy of the frontier molecular orbitals in the diagram of the three complexes is very similar because the fragments are isolobal. They have the same number of bonding orbitals and similar but not necessarily identical shapes and symmetries.

Figure 3 is an interaction diagram for the frontier molecular orbitals of the $[Pt_3(\mu\text{-}CO)_3(PH_3)_3]$ and $CuPH_3^+$ fragments. Similar results were obtained for $AuPH_3^+$ and $AgPH_3^+$. In the figure, the left and right sides correspond to the frontier levels of the platinum complex and $CuPH_3^+$, respectively. The center of the diagram corresponds to the molecular orbitals for the $[Pt_3(\mu\text{-}CO)_3(PH_3)_3]$–$CuPH_3^+$

Table 3 Main geometric parameters of the $[Pt_3(\mu\text{-}CO)_3(PH_3)_3]$–$MPH_3^+$ complex (M = Au, Ag, Cu)

System	Method	Pt–M	Pt–Pt	Pt–P	C–O	M–P	HPPt°	PMPt°	V(R_e)
$[Pt_3(\mu\text{-}CO)_3(PH_3)_3]$–$AuPH_3^+$	HF	292.3	275.3	237.1	112.4	238.4	117.7	116.7	−199.9
	MP2	269.8	263.0	228.5	117.1	225.7	117.4	116.8	−492.6
	B3LYP	284.9	273.3	233.7	115.7	231.8	117.2	117.3	−268.3
	PBE	280.8	270.5	231.7	117.1	229.3	118.4	117.6	−309.3
$[Pt_3(\mu\text{-}CO)_3(PH_3)_3]$–$AgPH_3^+$	HF	295.4	274.9	236.8	112.5	260.5	117.8	117.8	−162.5
	MP2	270.3	262.8	228.6	117.3	234.5	117.5	118.0	−411.0
	B3LYP	285.6	273.1	233.7	115.9	243.6	118.3	118.4	−230.9
	PBE	281.5	270.7	231.7	117.2	238.7	118.5	118.8	−265.9
$[Pt_3(\mu\text{-}CO)_3(PH_3)_3]$–$CuPH_3^+$	HF	273.8	274.9	237.1	112.4	238.7	117.8	117.7	−190.8
	MP2	253.3	262.3	228.9	117.2	212.7	117.4	118.1	−421.5
	B3LYP	272.9	264.5	233.8	115.7	222.7	118.2	118.3	−268.6
	PBE	260.9	270.3	231.8	117.2	219.7	118.4	118.7	−309.6
$[Pt_3(\mu\text{-}CO)_3(PCy_3)_3]$–$AuPCy_3^+$ [5]	Exp	275.8	270.8	227.3		227.0			
$[Pt_3(\mu\text{-}CO)_3(PPh_3)_3]_2$–$Au^+$ [12]	Exp	272.8	268.3						
$[Pt_3(\mu\text{-}CO)_3(PPh_3)_3]_2$–$Ag^+$ [12]	Exp	283.6	266.6						
$[Pt_3(\mu\text{-}CO)_3(P^iPr_3)_3]$–$CuP^iPr_3^{+a}$ [12]	Exp	260.4	267.1						

Distances in pm and angles in degrees at different levels of calculation. The interaction energy V(R_e) is shown with BSSE (kJ/mol)

[a] P $^iPr_3$ is tribulkytertiary phosphine

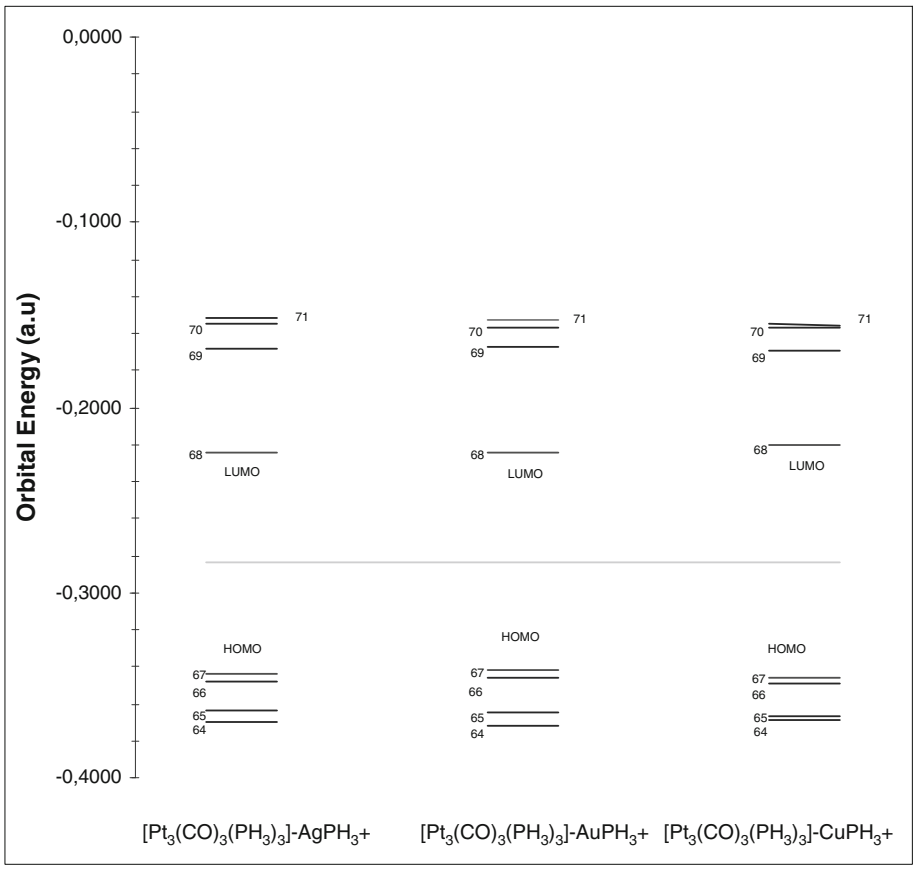

Fig. 2 The orbital energies of $[Pt_3(\mu\text{-}CO)_3(PH_3)_3]$–$MPH_3^+$ (M = Au, Ag, Cu)

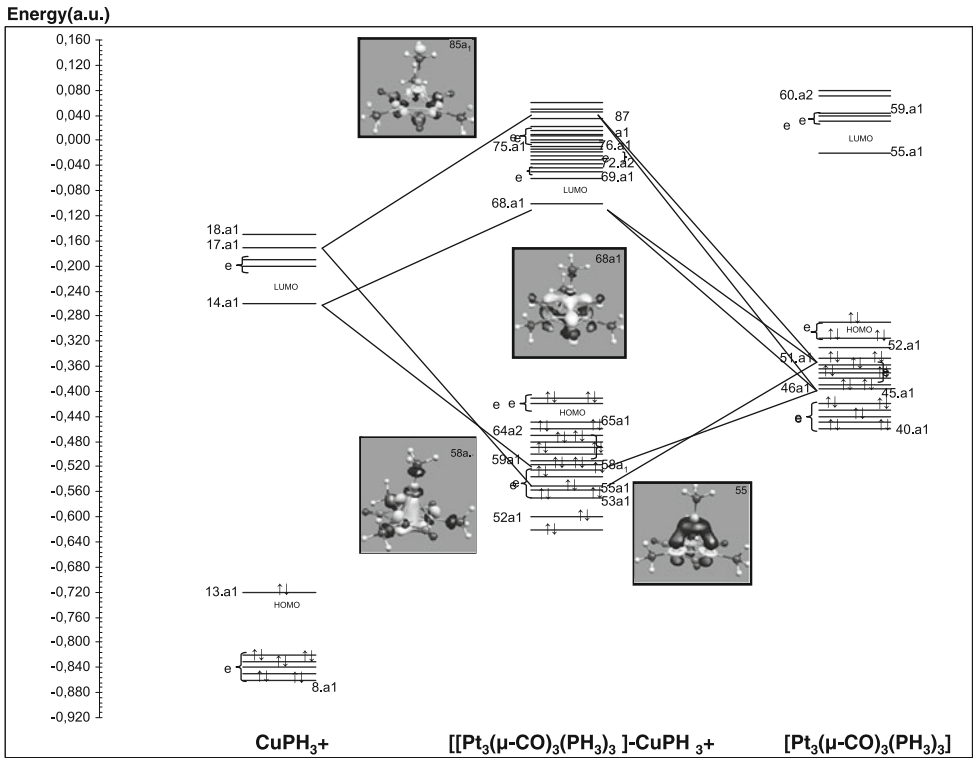

Fig. 3 Orbital energy diagram for the $[Pt_3(\mu\text{-}CO)_3(PH_3)_3]$–$CuPH_3^+$ complex

complex. Four orbitals show a strong interaction: $55a_1$, $58a_1$, $68a_1$, and $85a_1$, whereas the molecular orbitals remain unchanged. The orbitals generate the bonding ($55a_1$, $58a_1$) and antibonding ($68a_1$, $85a_1$) sigma levels from dz^2 (Pt) and dsp (Cu), respectively. These results clearly indicated a net effect of bonding through the orbital interactions. This magnitude is associated with covalent bonds.

Table 4 shows the natural bond orbital (NBO) population analysis based on the MP2 density of the complexes. Where atomic charges can be distinguished, we see that the Au charge (+0.426) in the $[Pt_3(\mu\text{-}CO)_3(PH_3)_3]$–$AuPH_3^+$ system decreases compared to the Au-free electrophilic $AuPH_3^+$ (+0.646), which indicates that Au is accepting electrons from the Pt_3 moiety. In contrast, the Pt charge (−0.025) in the system increases compared to the free $[Pt_3(\mu\text{-}CO)_3(PH_3)_3]$ (−0.006) cluster, where Pt is gaining electrons. A similar situation is seen when the electrophiles are Cu and Ag. The charge is transferred from the $[Pt_3(\mu\text{-}CO)_3(PH_3)_3]$ system to the MPH_3^+ fragment in the $[Pt_3(\mu\text{-}CO)_3(PH_3)_3]$–$MPH_3^+$ complex. The charge flow comes from the carbonyls and phosphines and is greater when the electrophile is the Au fragment, followed by Cu and finally Ag. The gross population per atom shell shows changes in the bond between the metal fragments due to electronic transfer. Thus, real effect is a inductive charge transfer where the electrophilic unit withdraws charge from the Pt_3 core. The Pt_3 core then compensates for the electron deficiency by pulling charge from the ligands.

3.2 Reactivity of electrophilic fragments

Table 5 shows the global and local properties of the electrophile fragments. Electrophiles were analyzed from conceptual DFT using Eqs. 1–5 at the MP2 and B3LYP levels, where an order of hardness can be established for the electrophile fragments: Au<Cu<Ag. Experimentally, the order of formation is the same, Au>Cu>Ag, which indicates that gold is the most stable complex with the $[Pt_3(\mu\text{-}CO)_3(PH_3)_3]$ cluster. The electrophilicity index also indicates that the Au fragment is the most electrophilic of the three, indicating that it is a better electrons acceptor because it is more polarizable. The parameter in both methods changes due to different magnitudes of the frontier orbitals.

The local reactivity of electrophiles has been studied using the condensed Fukui function. At the B3LYP and MP2 levels, the following order of local reactivity Au>Cu>Ag is seen. The local electrophilicity index on the metal (ω_M^+) gives the same tendency. All this local reactivity is correlated with the interaction energy of $[Pt_3(\mu\text{-}CO)_3(PH_3)_3]$–$MPH_3^+$. Table 3 shows that the energy of formation of the complex at the theoretical levels follows the Au>Cu>Ag trend.

Table 4 NBO analysis of the MP2 density for $[Pt_3(\mu\text{-}CO)_3(PH_3)_3]$–$MPH_3^+$, $[Pt_3(\mu\text{-}CO)_3(PH_3)_3]$ and MPH_3^+ complexes (M = Au, Ag, Cu)

System	Atom	Natural	Natural electron configuration
$[Pt_3(\mu\text{-}CO)_3(PH_3)_3]$–$AuPH_3^+$	Au	+0.426	$6S^{0.70}\ 5d^{9.85}\ 7p^{0.01}$
	Pt	−0.025	$6S^{0.64}\ 5d^{9.33}\ 6p^{0.01}\ 6d^{0.01}\ 8S^{0.01}$
	P	+0.263	$3S^{1.39}\ 3p^{3.28}\ 4S^{0.01}\ 3d^{0.05}\ 4p^{0.02}$
	C	+0.406	$2S^{1.29}\ 2p^{2.22}\ 3S^{0.03}\ 3p^{0.04}\ 3d^{0.01}$
	O	−0.588	$2S^{1.69}\ 2p^{4.87}\ 3d^{0.02}$
	P	+0.015	$3S^{1.39}\ 3p^{3.34}\ 3d0^{.05}\ 4p^{0.02}$
$[Pt_3(\mu\text{-}CO)_3(PH_3)_3]$–$AgPH_3^+$	Ag	+0.642	$5S^{0.41}\ 4d^{9.94}\ 6d^{0.01}\ 7p^{0.01}$
	Pt	−0.042	$6S^{0.65}\ 5d^{9.34}\ 6p^{0.01}\ 6d^{0.01}\ 8S^{0.01}$
	P	+0.258	$3S^{1.39}\ 3p^{3.28}\ 4S^{0.01}\ 3d^{0.05}\ 4p^{0.02}$
	C	+0.398	$2S^{1.29}\ 2p^{2.23}\ 3S^{0.03}\ 3p^{0.04}\ 3d^{0.01}$
	O	−0.589	$2S^{1.69}\ 2p^{4.87}\ 3d^{0.02}$
	P	+0.085	$3S^{1.43}\ 3p^{3.42}\ 3d^{0.04}\ 4p^{0.02}$
$[Pt_3(\mu\text{-}CO)_3(PH_3)_3]$–$CuPH_3^+$	Cu	+0.614	$4S^{0.42}\ 3d^{9.94}\ 4p^{0.01}\ 5p^{0.01}\ 5d^{0.01}$
	Pt	−0.043	$6S^{0.65}\ 5d^{9.34}\ 7S^{0.01}\ 6d^{0.01}\ 7p^{0.01}$
	P	+0.260	$3S^{1.39}\ 3p^{3.28}\ 4S^{0.01}\ 3d^{0.05}\ 4p^{0.02}$
	C	+0.398	$2S^{1.29}\ 2p^{2.23}\ 3S^{0.03}\ 3p^{0.04}\ 3d^{0.01}$
	O	−0.588	$2S^{1.69}\ 2p^{4.87}\ 3d^{0.02}$
	P	+0.101	$3S^{1.43}\ 3p^{3.41}\ 3d^{0.05}\ 4p^{0.01}$
$[Pt_3(\mu\text{-}CO)_3(PH_3)_3]$	Pt	−0.006	$6S^{0.64}\ 5d^{9.32}\ 7p^{0.02}$
	P	+0.276	$3S^{1.40}\ 3p^{3.25}\ 4S^{0.01}\ 3d^{0.05}\ 4p^{0.02}$
	C	+0.393	$2S^{1.31}\ 2p^{2.22}\ 3S^{0.03}\ 3p^{0.04}\ 3d^{0.01}$
	O	−0.628	$2S^{1.69}\ 2p^{4.91}\ 3p^{0.01}\ 3d^{0.02}$
$AuPH_3^+$	Au	+0.646	$6S^{0.47}\ 5d^{9.88}$
	P	+0.169	$3S^{1.38}\ 3p^{3.37}\ 4S^{0.01}\ 3d^{0.06}\ 4p^{0.02}$
$AgPH_3^+$	Ag	+0.859	$5S^{0.17}\ 4d^{9.97}\ 7p^{0.01}$
	P	−0.101	$3S^{1.44}\ 3p^{3.49}\ 4S^{0.01}\ 3d^{0.05}\ 4p^{0.02}$
$CuPH_3^+$	Cu	+0.829	$4S^{0.20}\ 3d^{9.96}\ 5p^{0.01}$
	P	+0.009	$3S^{1.43}\ 3p^{3.48}\ 4S^{0.01}\ 3d^{0.05}\ 4p^{0.01}$

Table 5 Global and local chemical properties of the MPH_3^+ fragments (M = Au, Ag, Cu) from frontier orbitals

Fragment	Method	μ	η	ω	f_M^+	ω_M^+
$AuPH_3^+$	MP2	−10.48	5.73	9.58	0.519	4.97
	B3LYP	−11.10	2.45	25.14	0.955	24.01
$AgPH_3^+$	MP2	−10.24	5.89	8.90	0.357	3.18
	B3LYP	−10.76	2.70	21.42	0.358	7.67
$CuPH_3^+$	MP2	−10.58	5.76	9.72	0.426	4.14
	B3LYP	−10.65	2.61	21.72	0.436	9.47

All values in eV

4 Conclusions

The $[Pt_3(\mu\text{-}CO)_3(PH_3)_3]$–$MPH_3^+$ (M = Au, Ag, Cu) complexes are stable at several levels of the theory. It is concluded that the equilibrium distances and interaction energy correspond essentially to an orbital interaction in the magnitude of a covalent bond. The analysis of bonding and antibonding orbitals accounts for such interaction. The charge transfer is mainly due to the carbonyl and the phosphine, while platinum atoms and electrophiles receive charge. According to the Fukui and electrophilicity local indices, stability in the series increases from Ag to Cu to Au. The formation energy of the complex at the theoretical levels follows the same trend, which reproduces the experimental results.

Acknowledgments This research was financed by FONDECYT under Project 1100162 (Conicyt-Chile) and Project Millennium P07-006-F. D.D. has a National Doctoral Fellowship (CONICYT D-21.070.206) and support for the implementation of the Doctoral Thesis no. 24.090.116. We value and appreciate the comments of the referees who read the original manuscript.

References

1. Imhof D, Venanzi LM (1994) Chem Soc Rev 23:185–193
2. Evans DG, Hallam MF, Mingos DMP, Wardle RWM (1987) J Chem Soc Dalton Trans 9:1889–1895

3. Chatt J, Chini P (1970) J Chem Soc A 5:1538–1541
4. Moor A, Pregosin PS, Venanzi LM (1982) Inorg Chim Acta 61:135–140
5. Braunstein P, Freyburger S, Bars O (1988) J Organomet Chem 352:C29–C33
6. Stockhammer A, Dahmen K-H, Gerfin T, Venanzi LM, Gramlich V, Petter W (1991) Helvetica Chimica Acta 74:989–992
7. Hao L, Xiao J, Vittal JJ, Puddephat RJ, Manojlović-Muir L, Muir KW, Torabi AA (1996) Inorg Chem 35:658–666
8. González-Moraga G (ed) (1993) Cluster chemistry. Spring, New York
9. Braunstein P, Rosé J (1988) Stereochemistry of organometallic and inorganic compounds, vol III. Elsevier, Amsterdam
10. Ranachandran R, Puddephatt RJ (1993) Inorg Chem 32:2256–2260
11. Burrows AD, Mingos DMP (1996) Coord Chem Rev 154:19–69
12. Pyykkö P (1997) Chem Rev 97:597–636
13. Pyykkö P (2004) Angew Chem Int Ed 43:4412–4456
14. Albinati A, Dahmen K-H, Demartin F, Forward JM, Longley CJ, Mingos DMP, Venanzi LM (1992) Inorg Chem 31:2223–2229
15. Gilmour DI, Mingos DMP (1986) J Organomet Chem 302: 127–146
16. Mingos DMP, Slee T (1990) J Organomet Chem 394:679–698
17. Evans DG (1988) J Organomet Chem 352:397–413
18. Mendizabal F, Donoso D, Olea-Azar C, Mera R (2007) Theochemistry 803:39–44
19. Mendizabal F, Olea-Azar C, Miranda S (2007) Int J Quantum Chem 107:1454–1458
20. Parr RG, Donnelly RA, Levy M, Palke WE (1978) J Chem Phys 68:3801–3807
21. Parr RG, Yang W (1989) Density functional theory for atoms and molecules. Oxford Press, New York
22. Parr RG, Pearson RG (1983) J Am Chem Soc 105:7512–7516
23. Parr RG, von Szentpaty L, Liu S (1999) J Am Chem Soc 121:1922–1924
24. Parr RG, Pearson R (1984) J Am Soc 106:4049–4050
25. Riedel S, Pyykkö P, Mata RA, Werner H-J (2005) Chem Phys Lett 405:148–152
26. Frisch MJ, Trucks GW, Schlegel HB, Gill PMW, Johnson BG, Robb MA, Cheeseman JR, Keith KT, Petersson GA, Montgomery JA, Raghavachari K, Al-Laham MA, Zakrzewski VG, Ortiz JV, Foresman JB, Cioslowski J, Stefanov BB, Nanayakkara A, Challacombe M, Peng CY, Ayala PY, Chen W, Wong MW, Andres JL, Replogle ES, Gomperts R, Martin RL, Fox DJ, Binkley JS, Defrees DJ, Baker J, Stewart JP, Head-Gordon M, Gonzalez C, Pople JA (2003) Gaussian 03, Inc, Pittsburgh
27. Møller C, Plesset MS (1934) Phys Rev 46:618–622
28. Perdew JP, Burke K, Ernzerhof M (1996) Phys Rev Lett 77:3865–3868
29. Christiansen P, Ermler W, Pitzer K (1985) Ann Rev Phys Chem 36:407–432
30. Andrae M, Heisserman M, Dolg M, Stoll H, Preuss H (1990) Theor Chim Acta 77:123–141
31. Bergner A, Dolg M, Küchle W, Stoll H, Preuss H (1993) Mol Phys 80:1431–1441
32. Huzinaga S (1965) J Chem Phys 42:1293–1301
33. Chattaraj PK, Roy DR (2006) Chem Rev 106:2065–2091
34. Albinati A (1977) Inorg Chimica Acta 22:L31–L32
35. Briant C, Wardle R, Mingos M (1994) J Organomet Chem 267:C49–C51